Exchange Enhancement of the Electron–Phonon Interaction: The Case of Weakly Doped Two-Dimensional Multivalley Semiconductors

Betül Pamuk, Paolo Zoccante, Jacopo Baima, Francesco Mauri, Matteo Calandra

Exchange Enhancement of the Electron-Phonon Interaction: the Case of Weakly Doped Two-Dimensional Multivalley Semiconductors

Betul Pamuk[1], Paolo Zoccante[2], Jacopo Baima,[2], Francesco Mauri[3,4] and Matteo Calandra[2]

[1]*School of Applied and Engineering Physics, Cornell University, Ithaca, New York 14853, USA*

[2]*Sorbonne Universités, UPMC, CNRS-UMR 7588, Institut des NanoSciences de Paris, F-75005, Paris, France*

[3] *Dipartimento di Fisica, Universitá di Roma La Sapienza, Piazzale Aldo Moro 5, I-00185 Roma, Italy*

[4] *Graphene Labs, Fondazione Istituto Italiano di Tecnologia, Italy*

The effect of the exchange interaction on the vibrational properties and on the electron-phonon coupling were investigated in several recent works. In most of the case, exchange tends to enhance the electron-phonon interaction, although the motivations for such behaviour are not completely understood. Here we consider the class of weakly doped two-dimensional multivalley semiconductors and we demonstrate that a more global picture emerges. In particular we show that in these systems, at low enough doping, even a moderate electron-electron interaction enhances the response to any perturbation inducing a valley polarization. If the valley polarization is due to the electron-phonon coupling, the electron-electron interaction results in an enhancement of the superconducting critical temperature. We demonstrate the applicability of the theory by performing random phase approximation and first principles calculations in transition metal chloronitrides. We find that exchange is responsible for the enhancement of the superconducting critical temperature in Li_xZrNCl and that much larger T_cs could be obtained in intercalated HfNCl if the synthesis of cleaner samples could remove the Anderson insulating state competing with superconductivity.

1. Introduction

Calculations of superconducting properties of materials require the knowledge of the electronic structure, the vibrational spectrum and a good description of the electron-phonon interaction. In state-of-the-art electronic structure approaches, density functional perturbation theory[1,2)] with local functionals (local density approximation or generalized gradient approx-

imation) is used. However, recently it has been shown that in several case the treatment of the electron-electron interaction in this framework is unsatisfactory and it becomes necessary to include a certain amount of exact exchange in the calculations. This is often the case in 2D or layered systems with weak Van der Waals out-of-plane interactions such as Graphene,[3,4] transition metal chloronitrides[5–8] or transition metal dichalcogenides.[9] However, enhancement of the electron-phonon coupling due to the electron-electron interaction has also been shown to occur in diamond[10] and in molecules like C_{60} in gas phase.[11,12] Despite all these recent calculations, there is not a clear understanding of when and why in a given system the exchange interaction or, more generally, the electron-electron interaction has important consequences for the electron-phonon coupling.

In the special case of a weakly doped multivalley two dimensional semiconductor, a more general picture of why the electron-electron interaction has important consequences in the renormalization of the electron-phonon coupling and of vibrational properties has been developed.[5–7] It relies on the general fact that at weak doping (few electrons/holes per valley) manybody effects enhance the response to any perturbation inducing a valley polarization. A physical realization of a multivalley 2D electron gas are Al/AS quantum wells. It has been shown that in this case a strain deformation acts as a *pseudo* magnetic field inducing a valley polarization , as it was shown in Ref.[13] Another form of a pseudo-magnetic field could be an intervalley phonon, namely a phonon with a momentum coupling two different valleys, inducing a change in the occupation of the valleys. In this case the pseudo magnetic field is simply the modulus of the deformation potential associated to this vibration. In all case, the response to the pseudo magnetic field is enhanced by the electron-electron interaction.

This effect can be justified by using a model Hamiltonian with SU($2g_v$) valley-spin symmetry,[14–16] with g_v being the number of valleys. This symmetry enforces the constrain that the interacting spin and valleys susceptibilities must be identical. As the spin susceptibility is enhanced by manybody effects in the low doping limit,[15] the same must occurs to the valley susceptibility. In real systems, the SU($2g_v$) symmetry holds for an isotropic mass tensor and at low doping. Indeed in this case, the Fermi momentum κ_F, as measured from the valley bottom, is much smaller than the valley separation and, consequently, the intravalley electron-electron interaction dominates over the intervalley one. This will be shown in more details in sec. 2.

A class of systems where these assumptions hold are the transition metal chloronitrides (examples are HfNCl and ZrNCl) that are semiconductors crystallizing in hexagonal structures and having almost perfect parabolic conduction bands at the high symmetry points **K**

and $2\mathbf{K}$. The interlayer interaction is extremely weak so that intercalation leads to an almost perfect realization of a 2D multivalley electron-gas.[5,17] Intercalation with alkali metals or alkaline earths induces a metal insulator transition at doping ranging from $x = 0.05$ to $x = 0.14$, depending on the system. In the metallic state and at low temperature a superconducting state occurs with T_c that can be as high as 25K.[18–21] The behaviour of T_c versus doping is very peculiar as T_c *decreases* with *increasing* doping, in contrast with their doping independent density of states (2D parabolic bands).[20] We will show in the sections below that this anomalous behaviour is due to the fact that the exchange interaction enhances the electron-phonon coupling in the low doping limit.

2. Spin and valley susceptibilities in a 2D multivalley electron gas

We consider a two dimensional multivalley electron gas composed by an isolated band partially filled with electrons, namely

$$H_0 = \sum_{\boldsymbol{\kappa} v \sigma} \frac{\hbar^2 \kappa^2}{2m^*} c^\dagger_{\boldsymbol{\kappa} v \sigma} c_{\boldsymbol{\kappa} v \sigma} \tag{1}$$

where $v = 1, ..., g_v$ is a valley index with g_v being the valley degeneracy, $\sigma = \pm$ is a spin index and c,$c^\dagger$ are fermion creation and destruction operators. The vector $\boldsymbol{\kappa}$ is measured from the bottom of each valley. In two dimensions, the Fourier transform of the electron-electron interaction within this band reads

$$v(q) = \frac{2\pi e^2}{\epsilon_M q} \tag{2}$$

where $\mathbf{q}$ is the exchanged momentum between the two interacting electrons, and the effect of the screening of other (empty) conduction and (filled) valence bands is included via the environmental dielectric constant ϵ_M. The electron-electron interaction has two contributions:

(i) The intravalley scattering with $q \sim \kappa_F$ (κ_F being the Fermi momentum measured from the valley bottom).

(ii) The intervalley scattering with $q \sim |\mathbf{K} - \mathbf{K}'| = |\mathbf{K}|$ where $\mathbf{K}$ and $\mathbf{K}' = 2\mathbf{K}$ are the positions of the valley bottoms in the Brillouin zone.

The intravalley contribution conserves the valley index of the electrons while the intervalley contribution does not.

In the low doping limit, namely for $\kappa_F \ll |\mathbf{K} - \mathbf{K}'|$, because of the divergence of the Coulomb repulsion for $q \to 0$, the intravalley scattering is dominant and the intervalley scattering can be neglected. Under this hypothesis, the valley and spin index are conserved by the Coulomb interaction. The valley index can then be treated as a pseudospin and the

manybody Hamiltonian has exact SU($2g_v$) spin and valley symmetry, namely (see e. g. Eq. 3.35 of Ref.[14])

$$\begin{aligned} H &= \sum_{\boldsymbol{\kappa}v\sigma} \frac{\hbar^2\kappa^2}{2m^*} c^\dagger_{\boldsymbol{\kappa}v\sigma} c_{\boldsymbol{\kappa}v\sigma} + \\ &+ \sum_{\boldsymbol{\kappa}v\sigma} \sum_{\boldsymbol{\kappa}'v'\sigma'} \sum_{\boldsymbol{q}} v(q) c^\dagger_{\boldsymbol{\kappa}v\sigma} c^\dagger_{\boldsymbol{\kappa}'v'\sigma'} c_{\boldsymbol{\kappa}'-\boldsymbol{q}v'\sigma'} c_{\boldsymbol{\kappa}+\boldsymbol{q}v\sigma} \end{aligned} \tag{3}$$

The Hamiltonian in Eq. 3 holds as long as (i) the screening of the other bands can be included in the environmental dielectric constant, (ii) intervalley scattering can be neglected. If these two conditions are satisfied, then it holds regardless of the number of valleys and of their position in the Brillouin zone.

As the Hamiltonian in Eq. 3 has exact SU($2g_v$) spin and valley symmetry, it follows that:

$$\chi_v = \chi_s \tag{4}$$

where the relation holds both for the interacting and non interacting susceptibilities. As a consequence, the knowledge of the interacting spin susceptibility is equivalent to the determination of the interacting valley susceptibility. In the absence of electron-electron interaction

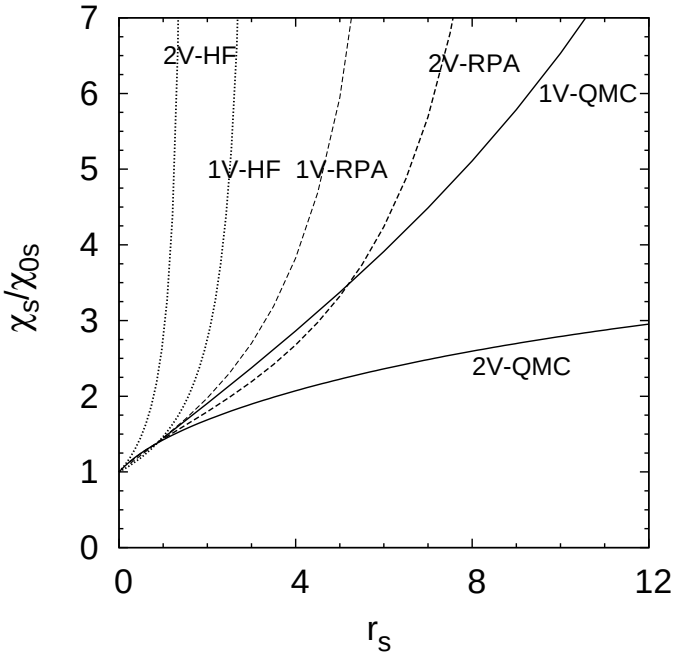

Fig. 1. Ratio between the interacting susceptibility calculated with several approximations and the bare susceptibility χ_{0s} for a two dimensional 1 (1V) and 2 (2V) valley electron gas as a function of $r_s = \frac{m^* e^2}{\epsilon_M \hbar^2 \sqrt{\pi n}}$ (HF= Hartree-Fock, RPA=Random Phase Approximation, QMC=Quantum Monte Carlo). Figure adapted with permission from Ref.[15] Copyrighted by the American Physical Society

the non interacting spin susceptibility is $\chi_{0s} = \mu_S N(0) = g_v m^*/\pi\hbar^2$ independent of doping and of the electron-gas parameter $r_s = \frac{m^* e^2}{\epsilon_M \hbar^2 \sqrt{\pi n}}$, with n being the electron-density .

The interacting spin susceptibility for a two dimensional two valley electron-gas has been calculated in detail Ref.[15] The results of this calculation are reported in Fig. 1. As it can be seen the Hartree Fock (HF) approximation leads to strongly divergent susceptibilities already at fairly low values of r_s, with the two valley case more divergent than the one valley case. This means that the exchange interaction leads to a magnetic solution. The Random Phase Approximation (RPA) removes the divergence, reduces the magnitude of the interacting spin susceptibility with respect to the HF case and leads to a smaller χ_s for the 2 valley electron-gas, in contrast to the HF result. The inclusion of correlation effects with the most accurate Quantum Monte Carlo (QMC) technique shows that correlation tends to reduce the exchange-induced enhancement in χ_S/χ_{0s}. Finally, it can be seen that for a 2 valley electron gas and $r_s < 2$, the RPA is an excellent approximation to the QMC results. As of Eq. 4, the same enhancement must occur in χ_v. In Fig. 2 we plot the interacting spin susceptibility for a two

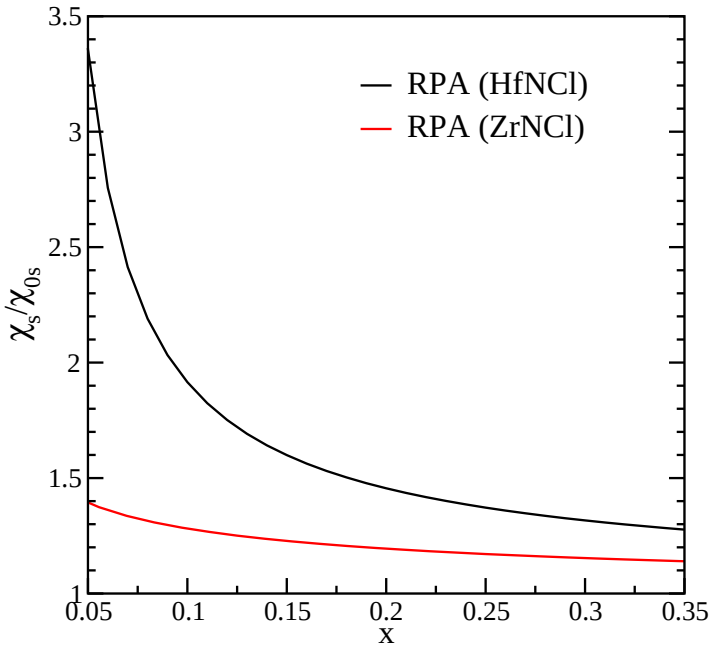

Fig. 2. (Color online) Ratio between the interacting susceptibility calculated in the Random phase approximation and the bare susceptibility χ_{0s} for a 2D 2 valley electron gas using relevant parameters of Li_xZrNCl and Li_xHfNCl. For Li_xZrNCl we use $\epsilon_M = 5.59$ and $m^* = 0.57m_e$, while for Li_xHfNCl we used $\epsilon_M = 4.93$ and $m^* = 0.615m_e$ where m_e is the electron mass. The larger divergence of the susceptibility in intercalated HfNCl is mostly due to the smaller environmental dielectric constant.

valley 2D electron-gas within the RPA (see supplemental materials of[5)] for more details), using relevant parameters for ZrNCl and HfNCl compounds.[5–7)] As it can be seen the spin susceptibility is enhanced at low doping and large $r_s = \frac{m^* e^2}{\epsilon_M \hbar^2 \sqrt{\pi n}}$ with respect to the doping-independent bare (non interacting) susceptibility. The enhancement is entirely due due to the electron-electron interaction. The enhancement of the spin susceptibility at low doping has been measured in Li_xZrNCl[20)]and it is in perfect agreement with RPA.[5)]

3. Electronic and vibrational properties of intercalated (Zr,Hf)NCl

3.1 Crystal structure

The primitive unit cell of intercalated (Zr,Hf)NCl has rhombohedral structure (space group $R\bar{3}m$, number 166) with 2 formula units per unit cell. It can also be constructed by a conventional cell of hexagonal structure with 6 formula units per cell with ABC stacking. It has been shown that the weak interlayer interaction,[5, 17, 22–24)] makes the stacking order negligible so that simulations with an hexagonal structure and AAA stacking (space group number 164) an 2 formula units unit cell leads to the same results.

3.2 Electronic structure

The electronic structure of intercalated (Zr,Hf)NCl using local functionals has been calculated by many authors.[5–8, 17, 25, 26)] The general agreement is that the charge transfer from alkali metals is complete and it acts as a rigid doping, so that it is appropriate to simulate these systems by using a uniform background doping. This has been explicitly verified both for the electronic and vibrational properties.[17)] Under this assumption, the electronic structure calculated using the generalized gradient approximation (GGA) approximation is shown in Fig. 3 (top). There are two parabolic bands at special points $\mathbf{K}$ and $\mathbf{K}' = 2\mathbf{K}$ of the Brillouin zone (BZ). The degree of trigonal warping is low and it increases by increasing doping, as shown in the Fermi surface projection on the k_x, k_y plane in Fig. 4. The effective mass of the band, in the generalized gradient approximation (GGA) within the PBE parametrization[27)] , is very close in the two compounds and weakly doping dependent. More details are given in Refs.[6, 7)]

The static HF exchange interaction can be included in the electronic structure calculation by using different flavour of hybrid functionals, as shown in Fig. 3 (bottom). Beside increasing the gap between valence and conduction band, the main effect of the exchange interaction is to slightly reduce the effective mass of the band (m^*).

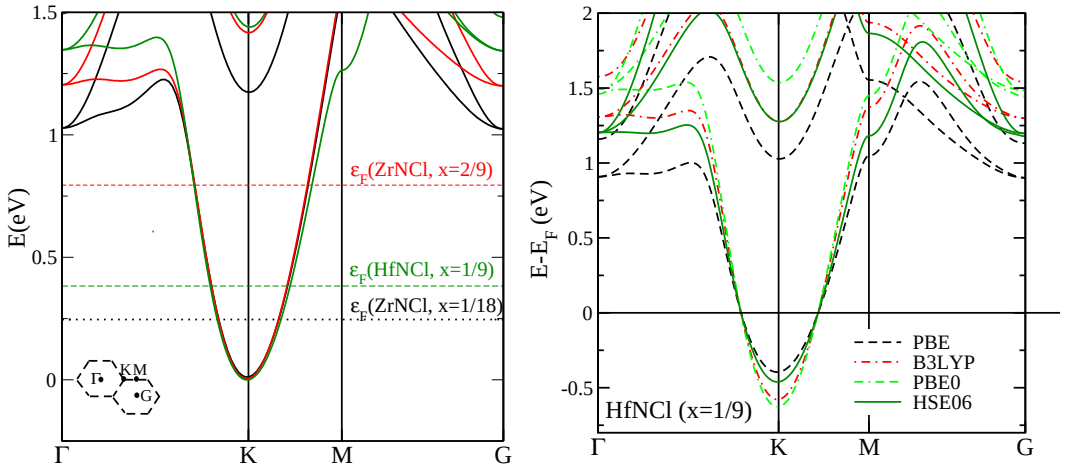

Fig. 3. (Color online) Top:electronic structure of intercalated (Zr,Hf)NCl for several doping (generalized gradiend approximation within the PBE parametrization[27]). Bottom:effect of the exchange interaction on the electronic structure of doped HfNCl at $x = 1/9$.

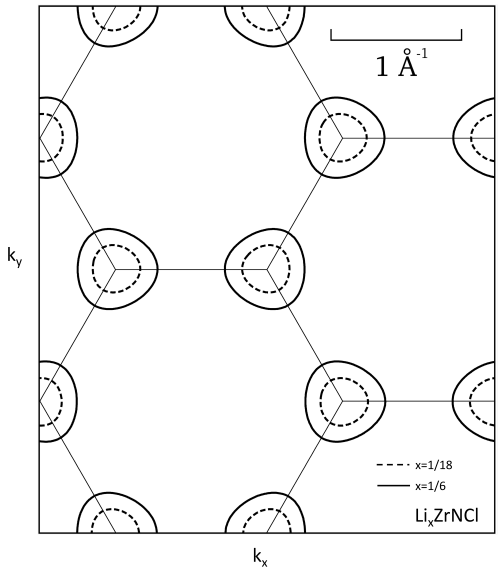

Fig. 4. In plane projection ($k_z = 0$) of the Li_xZrNCl Fermi surface as a function of doping.

3.3 Vibrational properties and electron-phonon interaction

The phonon dispersions of Li_x(Zr,Hf)NCl at the doping fraction of $x = 2/9$ calculated using Wannier interpolation as in Ref.[28] are shown in Fig. 5. The high energy modes are very similar in the two compounds, as shown in Fig. 5. These modes are composed of Nitrogen vibrations and are separated from all the others. Thus they are weakly affected by the

replacement of Zr with Hf. (Hf, Zr) and Cl modes are located in the low energy region below 40 meV. Hf modes are softened due to the larger Hf mass.

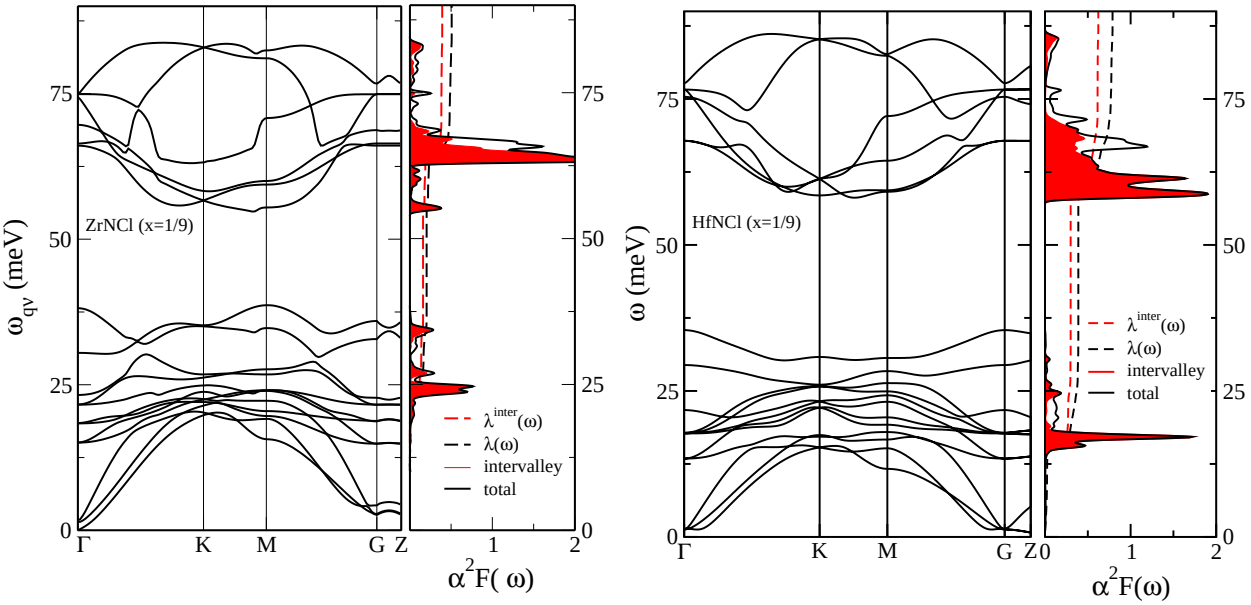

Fig. 5. (Color online) Phonon dispersion, Eliashberg function $\alpha^2F(\omega)$ and integrated Eliashberg function $\lambda(\omega)$ for Li_x(Zr,Hf)NCl at $x = 1/9$. The intervalley contribution to $\alpha^2F(\omega)$ and $\lambda(\omega)$ are also shown.

The electron-phonon coupling of a given mode ν at a phonon-momentum $\mathbf{q}$ reads:

$$\tilde{\lambda}_{\mathbf{q}\nu} = \frac{2}{\omega^2_{\mathbf{q}\nu} N(0) N_k} \sum_k |\tilde{d}^{\nu}_{\mathbf{k},\mathbf{k}+\mathbf{q}}|^2 \delta(\epsilon_{\mathbf{k}}) \delta(\epsilon_{\mathbf{k}+\mathbf{q}}), \tag{5}$$

where $\epsilon_{\mathbf{k}}$ is the quasiparticle energy of the partially occupied band. The electron-phonon matrix elements are defined such that $\tilde{d}^{\nu}_{\mathbf{k},\mathbf{k}+\mathbf{q}} = \langle \mathbf{k}|\delta\tilde{V}/\delta u_{\mathbf{q}\nu}|\mathbf{k}+\mathbf{q}\rangle$, $u_{\mathbf{q}\nu}$ is the phonon displacement of the mode $\omega_{\mathbf{q}\nu}$, and $\tilde{V}$ is the single particle potential that is fully screened by charge, spin, and valley exchange and correlation effects (see Eq. 2 in Ref.[5]) for more details). In the standard implementation of GGA/LDA functionals, there is no screening due to valley exchange effects and $\tilde{V}$ is simply the Kohn-Sham potential calculated with this approximation ($\tilde{V} = V_{KS}$).

The contribution of each mode to the electron-phonon interaction is better understood by looking at the Eliashberg function, namely:

$$\tilde{\alpha}^2F(\omega) = \frac{1}{2N_q} \sum_{\mathbf{q}\nu} \tilde{\lambda}_{\mathbf{q}\nu} \omega_{\mathbf{q}\nu} \delta(\omega - \omega_{\mathbf{q}\nu}) \tag{6}$$

and the integral $\tilde{\lambda}(\omega) = 2\int_0^{\omega} d\omega' \tilde{\alpha}^2F(\omega')/\omega'$.

We first calculate the electron-phonon interaction and the Eliashberg function using the GGA approximation. Then we decompose the electron-phonon coupling into intravalley and intervalley contributions. This can be easily done as the two valleys are located in different regions of the Brillouin zone and are disjoined. It is then sufficient to select the proper electron and phonon momenta involving only intra or intervalley scattering. The same decomposition is carried out on the Eliashberg function via Eq. 6.

At the GGA level, the Eliashberg function is composed of two main peaks, namely one at high energy due to N vibrations and mostly related to intervalley phonons (although a intravalley component is present) and a second one at lower energy mostly of intervalley character. The magnitude of the integrated total and intervalley electron-phonon couplings averaged over the Brillouin zone are shown in Fig. 5. It is clear that the electron-phonon interaction is dominated by intervalley phonons. The doping dependence of the electron phonon

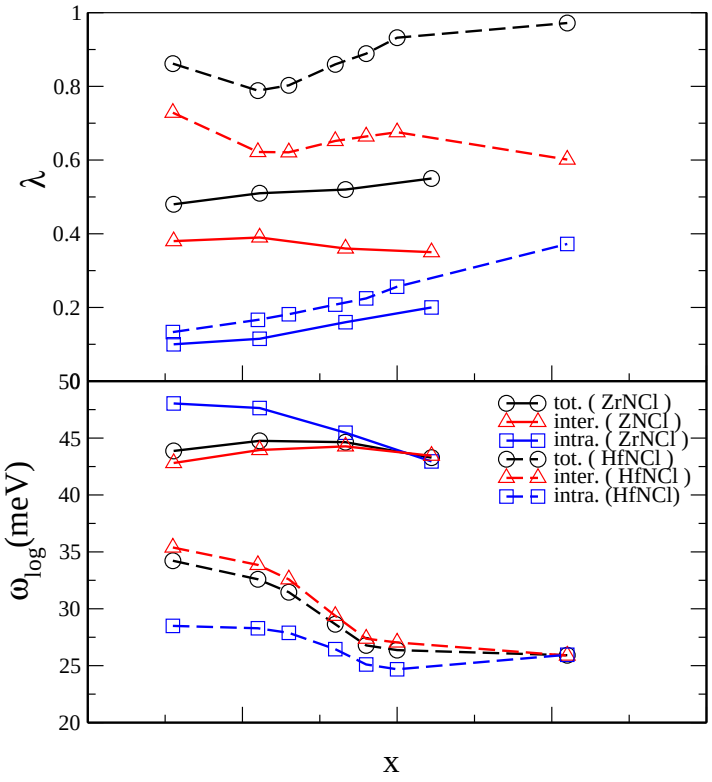

Fig. 6. (Color online) Electron-phonon coupling and logarithmic average of the phonon frequencies as a function of doping decomposed in the intervalley and intravalley contributions.

coupling is represented for the two systems in Fig. 6. The total electron-phonon coupling is almost twice as large in Li_xHfNCl than in Li_xZrNCl. This is mostly due to the increased intervalley electron-phonon interaction for the former compound. The intravalley coupling is

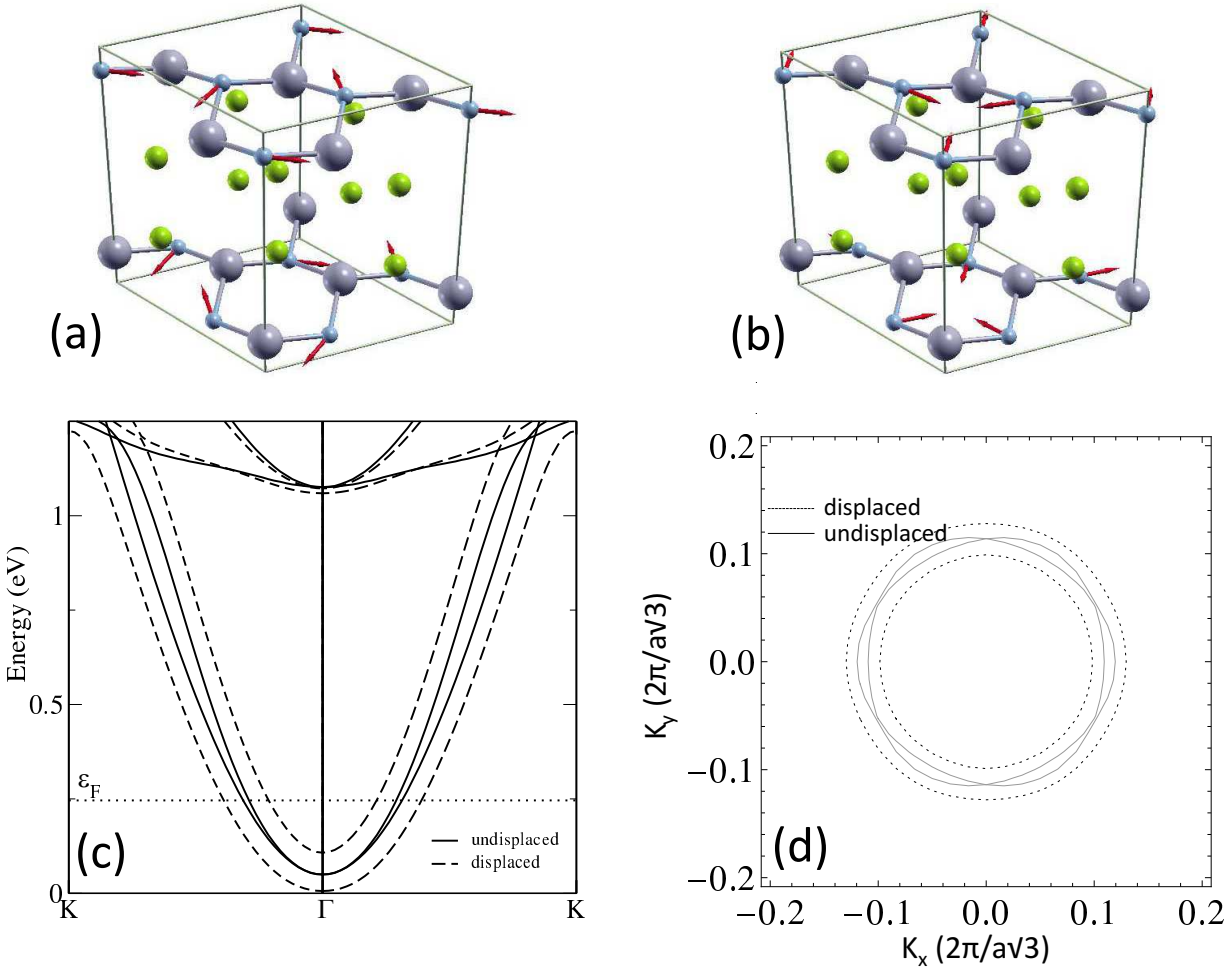

Fig. 7. (Color online) (a, b) Phonon pattern of the twofold degenerate intervalley phonon responsible for one of the prominent high-energy intervalley peaks in the Eliashberg function. The pattern is plotted in a $\sqrt{3} \times \sqrt{3}$ supercell. (Hf,Zr) big grey balls, Cl greenish balls and N cyan balls with arrows. The effect of the phonon patterns on the ZrNCl electronic structure (c) and Fermi surface (d) is shown in the bottom panels (c, d). The two valleys at **K** and **K′** in the Brillouin zone of the unit cell are folded at **Γ** in the Brillouin zone of the supercell. Intervalley phonons reduce the occupation of one valley and increase the occupation of the other one, acting as a pseudo-magnetic field on the valley degrees of freedom. Phonon displacements associated to other intervalley vibrations contributing to the electron-phonon interaction display an analogous behaviour.

roughly the same in both compounds.

As the band structures for the two compounds are very similar, the enhancement of the intervalley electron-phonon coupling is not due to a band structure effect, but it is partly due the larger deformation potential for intervalley phonons in HfNCl and partly due to the softening of the main peaks of the intervalley Eliashberg function in HfNCl and the consequent dependence ω^{-2} in λ^{inter}.

Given the dominant role of the intervalley electron-phonon interaction, it is interesting to

show the displacement pattern of these phonon modes and its effect on the electronic structure. For this reason, we consider a $\sqrt{3} \times \sqrt{3}$ supercell and we displace the atoms according to the patterns of the intervalley phonons generating the most prominent peaks in the intervalley Eliashberg function. We then calculate the electronic structure and Fermi surface for the displaced and undisplaced atomic configurations. There are several intervalley phonon modes contributing to $\alpha^2F(\omega)$, both at low energy and high energy. As they have qualitatively similar effects on the electronic structure, we just show in Fig. 7 (a,b) the action of the twofold degenerate high-energy mode mostly involving N vibrations.

The effect of intervalley vibrations on the electronic structure is to induce an unbalance in the occupation of the two valleys, as shown in Fig.7. This means that each intervalley phonon acts as a pseudo magnetic field on the valley degrees of freedom. In more details, if we assume a constant intravalley electron-phonon matrix element ($|d^{\nu}_{\mathbf{k},\mathbf{k}+\mathbf{K}}| \approx |d^{\nu}_{\mathbf{K},\mathbf{2K}}|$), the action of a small phonon displacement $u_{\mathbf{K}\nu}$ on the electronic structure can be described by the following one body Hamiltonian in the basis formed by the 2-component spinors $|\mathbf{K}+\boldsymbol{\kappa}\rangle$ and $|2\mathbf{K}+\boldsymbol{\kappa}\rangle$, with $\boldsymbol{\kappa} = \mathbf{k} - \mathbf{K}$:

$$H^{\nu}_{\boldsymbol{\kappa}} = \frac{\hbar^2\kappa^2}{2m^*}\hat{I} + B^{\nu}_{\mathrm{ext}}\mu_S\hat{\sigma_x}, \tag{7}$$

where $\hat{I}$ and $\hat{\sigma_x}$ are the 2×2 identity and the Pauli matrix along the x-direction, respectively, $B^{\nu}_{\mathrm{ext}} = |d^{\nu}_{\mathbf{K},\mathbf{2K}}|u_{\mathbf{K}\nu}/\mu_S$

As it happens in the magnetic case for χ_s, the response to the pseudo magnetic field, χ_v, is enhanced by the intervalley exchange-correlation, as predicted by Eq. 4. This effect is however absent in our DFT calculation, due to the lack of dependence of the exchange correlation functional on intervalley densities (see Supplemental of[5)] for more details), but it is normally present in hybrid-functional calculations via the dependence of the exact exchange on electronic wavefunctions.[6,7)]

As the total magnetization due to the pseudo magnetic field B^{ν}_{ext} is written either as $M = \chi_s B^{\nu}_{\mathrm{ext}}$ or as $M = \chi_{0s}\widetilde{B}^{\nu}$, where now $\widetilde{B}^{\nu}$ is the total magnetic field, sum of the external plus the exchange-correlation field, we have,

$$\frac{\widetilde{B}^{\nu}}{B^{\nu}_{\mathrm{ext}}} = \frac{|\widetilde{d}^{\nu}_{\mathbf{K},\mathbf{2K}}|}{|d^{\nu}_{\mathbf{K},\mathbf{2K}}|} = \frac{\chi_s}{\chi_{0s}} \tag{8}$$

namely the electron-phonon coupling at $\mathbf{q} = \mathbf{K}$ is renormalized by the electron-electron interaction exactly in the same way as the spin susceptibility with an enhancement that is independent from the phonon index ν. Assuming again a constant intervalley matrix element we

have that:

$$\tilde{\lambda}^{\text{inter}} = \left(\frac{\chi_s}{\chi_{0s}}\right)^2 \lambda^{\text{inter}} \tag{9}$$

so that $\tilde{\lambda} = \lambda^{\text{intra}} + \tilde{\lambda}^{\text{inter}}$. Thus the total electron-phonon interaction is enhanced in a way that is proportional to the ratio between the fully interacting valley susceptibility and the non interacting one. The occurrence of this effect in ZrNCl and HfNCl can be explicitly verified by using hybrid functional calculations with different components of exact exchange.[6,7] In the framework of our RPA model we can just renormalize the intervalley electron-phonon interaction with the ration of the χ_s/χ_{0s} in Fig. 1.

4. Conclusions

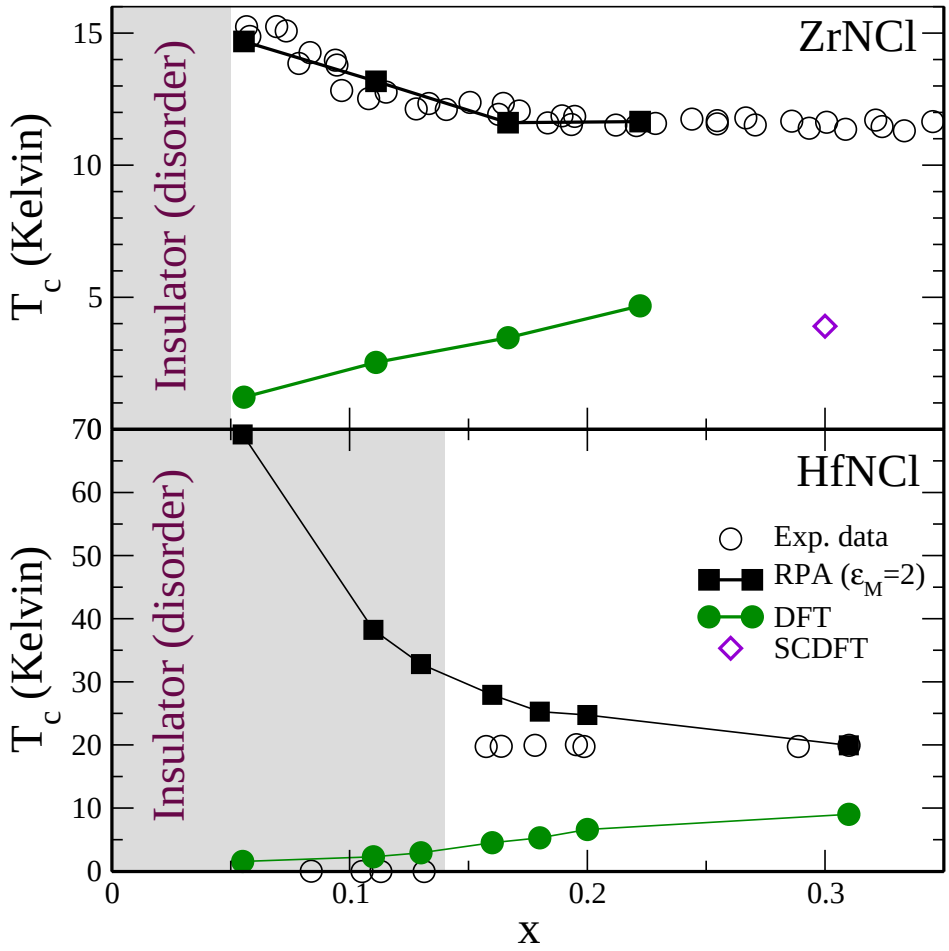

Fig. 8. (Color online) Superconducting critical temperatures calculated with different approximations and compared with experiments.[21,29] The grey region marks the occurrence of an insulating region detected in experiments and due to disorder (Anderson transition).

The superconducting properties for both compounds as a function of doping/intercalation are shown in Fig. 8. In experiments, a metal insulator transition occurs at low doping due to the occurrence of disorder. In intercalated HfNCl the Anderson insulating state persists to doping as large as $x = 0.14$, hindering the detection of a T_c enhancement in HfNCl.

Density functional theory calculations based on gradient corrected functionals lead to an estimate of T_c[30] that is too low compared to experiments and it also has the incorrect behaviour of T_c versus doping. Indeed within the PBE parametrization,[27] T_c *increases* by *increasing* doping. Electron-electron interaction included within the RPA and via renormalization of the intervalley electron-phonon interaction leads to the correct T_c versus doping behaviour and, for the case of Li_xZrNCl, to an excellent agreement with experiments. In HfNCl the comparison with experiments is complicated by the more persistent Anderson transition and the difficulties of obtaining very good ordered samples in the low doping limit. Our results predict that removal of the Anderson transition or better control of doping in Li_xHfNCl could lead to emergence of a high T_c superconducting state.

5. Acknowledgments

We acknowledge Stefania de Palo for providing us the data in Fig. 1. We acknowledge support from the acknowledge support from the European Union Horizon 2020 research and innovation program under Grant agreement No. 696656-GrapheneCore1 and from Agence Nationale de la Recherche under the reference No. ANR- 13-IS10-0003-01. Computer facilities provided by CINES, IDRIS, and CEA TGCC (Grant EDARI No. 2017091202) and the institute for computing and data sciences (ISCD) at UPMC based in France. B. P. acknowledges National Science Foundation [Platform for the Accelerated Realization, Analysis, and Discovery of Interface Materials (PARADIM)] under Cooperative Agreement No. DMR-1539918 for her time at Cornell University.

References

1) P. Giannozzi, S. D. Gironcoli, P. Pavone, and S. Baroni: Phys. Rev. B **43** (1991) 7231.

2) X. Gonze and C. Lee: Phys. Rev. B **55** (1991) 10355.

3) M. Lazzeri, C. Attaccalite, L. Wirtz, and F. Mauri: Phys. Rev. B **78** (2008) 081406.

4) C. Attaccalite, L. Wirtz, M. Lazzeri, F. Mauri, and A. Rubio: Nano Lett. **10** (2010) 1172.

5) M. Calandra, P. Zoccante, and F. Mauri: Phys. Rev. Lett. **114** (2015) 077001.

6) B. Pamuk, J. Baima, R. Dovesi, M. Calandra, and F. Mauri: Phys. Rev. B **94** (2016) 035101.

7) B. Pamuk, F. Mauri, and M. Calandra: Phys. Rev. B **96** (2017) 024518.

8) Z. P. Yin, A. Kutepov, and G. Kotliar: Phys. Rev. X **3** (2013) 021011.

9) M. Hellgren, J. Baima, R. Bianco, M. Calandra, F. Mauri, and L. Wirtz: Phys. Rev. Lett. **119** (2017) 176401.

10) G. Antonius, S. Poncé, P. Boulanger, M. Côté, and X. Gonze: Phys. Rev. Lett. **112** (2014) 215501.

11) C. Faber, J. L. Janssen, M. Côté, E. Runge, and X. Blase: Phys. Rev. B **84** (2011) 155104.

12) J. Laflamme Janssen, M. Côté, S. G. Louie, and M. L. Cohen: Phys. Rev. B **81** (2010) 073106.

13) O. Gunawan, Y. P. Shkolnikov, K. Vakili, T. Gokmen, E. P. D. Poortere, and M. Shayegan: Phys. Rev. Lett. **97** 186404.

14) T. Ando, A. B. Fowler, and F. Stern: Rev. Mod. Phys. **54** (1982) 437.

15) M. Marchi, S. De Palo, S. Moroni, and G. Senatore: Phys. Rev. B **80** (2009) 035103.

16) S. D. Sarma, E. H. Hwang, and Q. Li: PRB **80** (2009) 121303(R).

17) R. Heid and K.-P. Bohnen: Phys. Rev. B **72** (2005) 134527.

18) S. Yamanaka, H. Kawaji, K. i. Hotehama, and M. Ohashi: Adv. Mater. **8** (1996) 771.

19) S. Yamanaka, K. Hotehama, and H. Kawaji: Nature (London) **392** (1998) 580.

20) Y. Taguchi, A. Kitora, and Y. Iwasa: Phys. Rev. Lett. **97** (2006) 107001.

21) T. Takano, T. Kishiume, Y. Taguchi, and Y. Iwasa: Phys. Rev. Lett. **100** (2008) 247005.

22) Y. Kasahara, T. Kishiume, K. Kobayashi, Y. Taguchi, and Y. Iwasa: Phys. Rev. B **82** (2010) 054504.

23) T. Takano, Y. Kasahara, T. Oguchi, I. Hase, Y. Taguchi, and Y. Iwasa: J. Phys. Soc. Jpn. **80** (2011) 023702.

24) A. S. Botana and W. E. Pickett: Phys. Rev. B **90** (2014) 125145.

25) R. Weht, A. Filippetti, and W. E. Pickett: Europhys. Lett. **48** (1999) 320.

26) R. Akashi, K. Nakamura, R. Arita, and M. Imada: Phys. Rev. B **86** (2012) 054513.

27) J. P. Perdew, K. Burke, and M. Ernzerhof: Phys. Rev. Lett. **77** (1996) 3865.

28) M. Calandra, G. Profeta, and F. Mauri: Phys. Rev. B **82** (2010) 165111.

29) Y. Kasahara, T. Kishiume, T. Takano, K. Kobayashi, E. Matsuoka, H. Onodera, K. Kuroki, Y. Taguchi, and Y. Iwasa: Phys. Rev. Lett. **103** (2009) 077004.

30) We calculate the superconducting critical temperature using the McMillan-Allen-Dyndes equation using the values of λ and $\omega_{\log}$ obtained in this work and the screened pseudopotential $\mu^* = \mu/\left[1 + \mu \log(\epsilon_F/\omega_D)\right]$ with ϵ_F being the Fermi level and $\omega_D = 90$ meV. We set the unscreened pseudopotential for doped HfNCl (ZrNCl) at $\mu = 0.231$ ($\mu = 0.198$) giving the correct estimate of the experimental at the highest doping of $x = 0.31$ ($x = 2/9$) by using the RPA enhanced fully screened electron-phonon coupling $\tilde{\lambda}$. These value is close to the GW estimates of 0.237 (0.203) at $x = 0.31$ ($x = 0.1$) for doped HfNCl (ZrNCl)[26)]

31) W. L. McMillan: Phys. Rev. **167** (1968) 331.

32) P. B. Allen and R. C. Dynes: Phys. Rev. B **12** (1975) 905.